BL-14B/2020G585

X-ray topography of crystallographic defects in wide-bandgap semiconductors using a high-resolution digital camera

Yongzhao YAO[1,*] Yoshihiro SUGAWARA[1], Yukari ISHIKAWA[1], and Keiichi HIRANO[2]
[1] Japan Fine Ceramics Center,
2-4-1 Mutsuno, Atsuta, Nagoya, Aichi 456-8587, Japan
[2] Photon Factory, Institute of Materials Structure Science,
High Energy Research Organization,
1-1 Oho, Tsukuba, Ibaraki 305-0801, Japan

1 Introduction

A high-resolution CMOS camera equipped with a scintillator and relay lenses was used to record X-ray topographic (XRT) images of wide-bandgap semiconductor wafers, including 4H-SiC, GaN, AlN, and β-Ga_2O_3. The images were compared with those recorded with nuclear emulsion plates (NEPs) and a CCD camera at the same sample site. Fine structures of dislocation contrasts, which allowed for accurate identification of the dislocation types, could be observed using the CMOS camera. The results suggest that the CMOS camera can provide high-quality images that are comparable with the NEPs; hence, the reported approach is a promising one for real-time dislocation observation in power devices under operation. [1]. This report is based on the data published in ref. [1].

2 Experiment

Commercial (0001)-face 4H-SiC, (0001)-face GaN [2], (0001)-face AlN [3,4], and (-201)-face β-Ga_2O_3 wafers [5] were investigated. The GaN wafer has dislocation density ~10^7 cm^{-2}, and the other three wafers had dislocation densities in the order of 10^4 cm^{-2}.

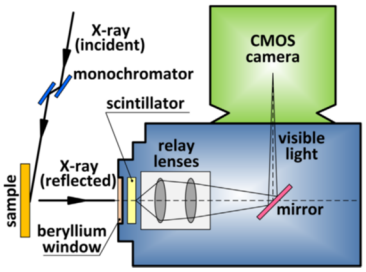

Fig. 1: Schematic of the optic system used to record XRT images [1].

XRT experiments were carried out at BL-14B (KEK-PF). The original beam size is about 9 mm×16 mm. Grazing-incidence mode with an incident angle of ~5° was used for all measurements. The reciprocal lattice vectors (g-vectors) used to acquire the XRT were 11-28 for 4H-SiC, 11-26 for GaN, 11-24 for AlN, and -626 for β-Ga_2O_3. The wavelength of the monochromatic X-ray was adjusted with the range of 0.84 Å–1.36 Å in accordance with the g-vectors. Fig. 1 shows a schematic illustration of the experimental setup. The X-rays reflected from the sample reached the scintillator surface and visible light with a wavelength of λ=520–535 nm was then emitted from the backside of the scintillator. The scintillator was fabricated with the fluorescent materials LuAG:Ce ($Lu_3Al_5O_{12}$:Ce+) or GAGG:Ce ($Gd_3Al_2Ga_3O_{12}$:Ce+) and had a thickness of ~50 μm. This thickness was optimized to account for the trade-off between the spatial resolution and luminescence efficiency. After passing through 10× relay lenses with a numerical aperture (NA) of 0.3 (or 20×, NA=0.4), the visible light was directed to the CMOS camera (Hamamatsu ORCA-Flash 4.0 V3) using a mirror. The camera consisted of a detector with 2048×2048 pixels (6.5 μm×6.5 μm/pixel). When the 10× relay lenses were used, the optic system provided an effective spatial resolution of ~0.65 μm for the original topograph. The maximum size of a single image corresponds to a 1.3 mm×1.3 mm area on the sample surface, which in most cases is sufficiently wide to cover the entire electrode area of a real device. Images of wider areas can be created by stitching together grid images. The camera has a full capacity of 30,000 electrons per pixel and the read-out noise is 0.8 electron, leading to a dynamic range of ~37,000:1, which is much larger than that of NEPs. The read-out speed is 10 ms/frame. The above parameters enabled continuous 16-bit video recording at a speed of 100 frames/s. For comparison, two other recording media were also used for XRT image acquisition, NEPs (Polysciences, Inc., Ilford NEP L4, 25 μm) and a CCD camera (Photonic Science Ltd., XFDI 40 mm). The CCD camera had sensor array of 1392×1040 pixels (24 μm×24 μm/pixel) and its effective dynamic range was >16,000:1. The sample-camera distance was the same for all three recording media [1].

3 Results and Discussion

To assess the spatial resolution of each recording medium, first, a 4H-SiC wafer with various types of dislocations was chosen. Fig. 2 shows a comparison of the XRT images acquired via CMOS, NEP, and CCD.

Negative images were obtained, i.e., the bright contrast corresponds to less X-ray exposure. Because of the comparatively lower spatial resolution, individual dislocations cannot be resolved from the CCD image. The large bright spots (hundreds of micrometers) are associated with dislocations that have a wide surrounding strain field. The Burgers vectors (***b***) of these dislocations typically have

a giant *c*-component (*n*c, n≥3) and may have a mixed-type character [6]. Arrays, if composed by threading screw dislocations (TSDs), can be faintly recognized from the CCD image. Compared with the CCD image, a much higher spatial resolution was achieved using the CMOS camera. The spot-like contrast associated with threading dislocations and arc-shaped contrast associated with basal plane dislocations (BPDs) were clearly revealed. Threading edge dislocations (TEDs) aligned as arrays could be well resolved as individual dislocations even though the distance between neighboring TEDs was only ~10 μm. This result indicated that a CMOS camera is useful for crystals with dislocation densities up to ~10^6 cm^{-2}, which is regarded as the resolution limit of the XRT technique. NEPs are generally considered as the best recording medium for XRT in terms of resolution [7]. Comparing Figs. 2(a) and 2(b), the results suggest that the CMOS camera can provide a similar resolution as NEP. Moreover, the CMOS camera appeared to be more powerful than the NEP for observation of a high-density BPD network near a threading dislocation (TD) with a giant ***b***. As shown in Fig. 2(b), the area containing such a BPD network has very poor contrast in the NEP image, which is because of the influence from the giant TD during development and fixation. In comparison, the BPD network could be clearly imaged using the CMOS camera because of the digital recording. Each pixel can be regarded as an isolated detector that responds only to the photons that reach the pixel area, and it is not influenced by the neighboring area. This gives the CMOS camera an advantage over analog NEPs for observing highly defective crystals.

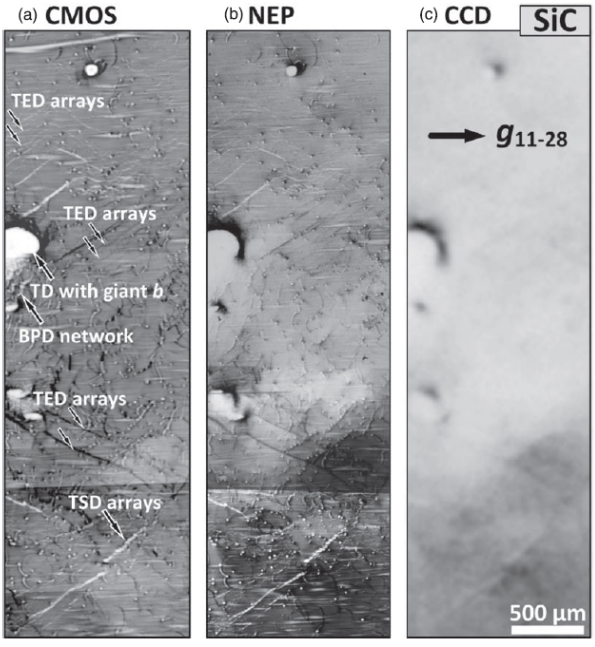

Fig. 2: XRT images of 4H-SiC taken with (a) CMOS, (b) NEP, and (c) CCD [1].

To further improve the resolution, the 10× relay lens was replaced with a 20× lens. The area of the scintillator projected to the detector decreased to 1/4 and the nominal resolution improved to 0.325 μm/pixel. Fig. 3 shows a comparison between the CMOS images with the 20× and 10× lenses and the NEP image. We focused on evaluating whether the images have sufficient spatial resolution to allow accurate assignment of the Burgers vector. In 4H-SiC, dislocations were generally grouped into BPDs and TDs, and they were further classified into TEDs, TSDs, and threading mixed dislocation (TMDs) with ***b***=*c*+*a*. As shown in Fig. 3, BPDs are revealed as arc-shaped or line-shaped contrasts. These contrasts appear as bright (or dark) lines with dark (or bright) edges on both sides, or as lines with asymmetric bright/dark edges, depending on the Burgers vector with respect to the g-vector. Judging from the bright/dark contrast and its symmetry, the Burgers vector of BPDs can be accurately determined.

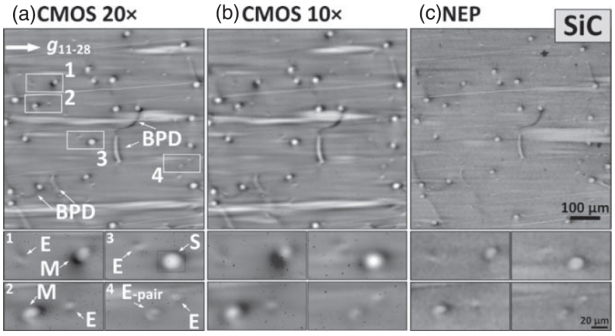

Fig. 3: XRT images of 4H-SiC taken with (a) CMOS with a 20× lens, (b) CMOS with a 10× lens, and (c) nuclear emulsion plate [1].

In the similar way, we have also confirmed that this recording technique is applicable to dislocation observation in GaN, AlN and β-Ga_2O_3 [1]. The results show that with a 10× lens, the CMOS camera had a similar resolution as that of NEP, and the resolution could be further improved by using a 20× lens. The fine structure of dislocation contrasts was observed, which allowed for accurate identification of the Burgers vectors. The results indicated that the proposed system is promising for real-time dislocation observation for power devices under operation.

Acknowledgement

One of the authors Y.Y. is grateful to Dr. Y. Takahashi for her kind instructions on experimental operations.

References

[1] Y. Yao, Y. Sugawara, Y. Ishikawa, and K. Hirano, Jpn. J. Appl. Phys. **60**, 010908 (2021).
[2] Y. Yao, et al., J. Electron. Mater. **49**, 5144 (2020).
[3] Y. Yao, et al., Appl. Phys. Lett., **117**, 092102 (2020).
[4] Z. G. Herro, et al., J. Cryst. Growth **312**, 2519 (2010).
[5] A. Kuramata, et al., Jpn. J. Appl. Phys. **55**, 1202A2 (2016).
[6] X. R. Huang, et al., Appl. Phys. Lett. **74**, 353 (1999).
[7] S. Yamaguchi, et al., Jpn. J. Appl. Phys. **58**, 060901 (2019).

* y_yao@jfcc.or.jp